Mechanical Behavior of Quenched Isotactic Polypropylene Crystallized by Thermal and Solvent Treatments

F. DE CANDIA, R. RUSSO, and V. VITTORIA, *Istituto di Richerche su Tecnologia dei Polimeri e Reologia, C.N.R., Via Toiano 6, 80072 Arco Felice, Naples, Italy*

Synopsis

Films of quenched isotactic polypropylene were either annealed at 80, 90, 100, 110°C for 30 min or kept in different liquids for 24 h at 25°C. The liquids were cyclohexane, chloroform, and carbon tetrachloride. Both treatments induce crystallization of quenched films and the development of crystallinity was detected by carrying out density and wide-angle x-ray scattering measurements. Small-angle light scattering experiments, performed on the starting and on the crystallized samples, show that in the zones in which spherulites are present the basic gross morphology does not change after the treatments, although the increase of crystallinity is substantial for all the samples. The analysis of the mechanical behavior also indicates the absence of relevant morphological changes following the different treatments. On the other hand the increased crystallinity strongly influences the complex structural and molecular rearrangement characterizing the transition from the spherulitic to the fiber morphology. The results are discussed in terms of the great significance that structural modifications have on the physical properties.

INTRODUCTION

Isotactic polypropylene (iPP) is a polymer of considerable commercial importance. Numerous studies have been undertaken on its crystal structure, mode of crystallization, and the properties of the various solid phases. It is well known that, when rapidly quenched from the melt, it forms a phase of intermediate order between amorphous and crystalline, variously described in literature as smectic, paracrystalline, or "condis crystal" (conformationally disordered crystal).[1-8]

The study of the smectic phase of iPP is particularly important from the technological point of view, since specimens of solid polypropylene, obtained under rapid cooling conditions, will always have a fraction of material in an intermediate state of order. At room temperature the smectic phase is stable for long periods of time, but it reverts to the monoclinic crystalline phase when heated at temperatures higher than 70°C.[9,10] The conversion to the crystalline form can cause dimensional instability and therefore influences the usefulness of the polymer. In the past many authors have studied the development of crystallinity and its kinetics, induced by thermal treatments on the quenched iPP. Recently we have shown that the smectic component of a quenched film can be transformed into the crystalline phase by solvent-induced crystallization (SINC) and investigated this process in different liquids.[11] Of all the liquids investigated, those that were found to be most effective in inducing the crystallization phenomenon were cyclohexane, carbon

Journal of Applied Polymer Science, Vol. 34, 689–701 (1987)
© 1987 John Wiley & Sons, Inc.
CCC 0021-8995/87/020689-13$04.00

tetrachloride, and chloroform. Solvent-induced crystallization is carried out at 25°C and provides an alternative mode of structure formation without increasing the temperature. Thermally and solvent-induced structure and morphologies, in systems which undergo such a modification, ought to be quite different, and a comparison of these two systems can be very interesting.[12-14] The analysis of mechanical behavior is one of the most useful approaches and it points up the great significance that structural modifications have on physical properties.[15] Furthermore, through the considerations of structure-mechanical properties relationships, much insight can be gained in terms of the morphology of the underlying material. We have therefore studied the mechanical behavior of films crystallized either thermally or by SINC, and attempted to relate the observed results with the structure of the films.

EXPERIMENTAL

Isotactic Polypropylene of Mw = 307,700 and Mn = 15,600 is a product of RAPRA (Great Britain). The steric purity was analyzed using ^{13}C NMR spectroscopy, and results gave 98.3% isotactic content. Starting films (S) were obtained by heating the iPP pellets at 200°C, pressing them into the film shape with a thickness of 0.02 cm and quickly cooling the melt in an acetone-dry ice bath at −70°C. The material obtained is a biphasic smectic-amorphous system with a density 0.883 g/cm^3 for which we determined an amorphous fraction of 53%.[16]

Different strips of the starting film were kept for 30 min at 80°C, 90°C, 100°C, and 110°C under nitrogen gas (samples A80, A90, A100, A110, respectively). For the solvent-induced crystallization process, the quenched films were immersed for 24 h in cyclohexane (sample CES), chloroform (CLS), and carbon tetrachloride (TCS) at 25°C. Upon removal from the liquids, the samples were dried under vacuum for 5 days at 25°C. Density measurements were performed by floating the sample in a mixture of 1,2-dimethoxy ethane and 2-ethoxy ethanol.

Wide-angle x-ray diffractograms (WAXD) were obtained by using a PW 1050 Philips powder diffractometer (CuKα Ni-filtered radiation). The scan rate used for the WAXS profiles was 0.5° min^{-1}.

Differential scanning calorimetry (DSC) was carried out over the temperature range 200–500°K using a Mettler differential scanning calorimeter, purged with nitrogen gas and chilled with liquid nitrogen. Runs were conducted on samples of about 15 mg at two different heating rates (20°C/min and 50°C/min).

Small-angle light scattering (SALS) experiments were performed utilizing a Spectra Physics model 162A Argon ion laser (λ = 4965 Å), scattering patterns were recorded on Polaroid Type 55 film.

To study the mechanical behavior the samples were drawn at a constant elongation rate of 1 cm/min in a uniaxial tensile testing instrument (Tensilon UTM-II Toyo Measuring Instruments). The measurements were performed at room temperature. Dumbbell samples were cut from the films, with a gauge length of 1 cm. Marks spaced 2 mm apart were placed on the samples and their displacement recorded photographically. The records were used to determine the local draw ratio λ_L as a function of the nominal draw ratio, λ_N, as determined from the displacement of the clamps. The elastic moduli were

determined from the slope of the initial part of the stress-strain curve within the linear trend. The values obtained were averaged over many measurements.

RESULTS

Density and X-Ray Diffraction

Both the temperature and the liquids induce crystallization of the quenched iPP, as demonstrated by the substantial increase in density as reported in Table I. A comparable level of conversion was obtained for the two sets of samples.

In Figure 1 the wide angle x-ray diffractograms of the starting sample and crystallized films are shown. The diffractogram of sample S shows the profile usually reported for the smectic form of iPP,[1] while for the other films the transformation of the smectic phase into the monoclinic form of iPP is evident. The reciprocal of the width at half-height of the (110) iPP reflection at 2θ 14° is reported in Table I for each sample. This parameter can be chosen as an index of order for the crystallized samples.[6] It is proportional to the crystallite dimension L, but its value is also influenced by lattice distortions.[17] A substantial increase in this parameter both for the thermally and for the solvent crystallized samples is evident with respect to the starting sample S. It increases on increasing the annealing temperature for the thermally crystallized samples and for the solvent crystallized samples it increases from CES to TCS and CLS.

A comparison between the density and the 1/A parameter for samples CLS and TCS shows that a higher 1/A parameter does not correspond to a higher density (TCS). This might be explained by the formation in the TCS sample of smaller or more defective crystallites; an alternative explanation is that the higher density of this sample is due to solvent entrapped in or between the crystallites.

Thermal Analysis

In Figure 2, we report the DSC runs for the samples heated at 50°C/min. These curves, together with the WAXD profiles, can help understand more clearly the crystallization from the smectic form to the monoclinic one. The results for the quenched form and for the thermally crystallized samples are in good agreement with those already reported for iPP.[8,10]

TABLE I
Density (g/cm^3) and Reciprocal of the Half-Height Width of the (110) Diffraction Peak at 2θ = 14° for the Analyzed Samples

Sample	Density (g/cm^3)	1/A (degrees^{-1})
S	0.883	0.23
A80	0.890	0.44
A90	0.894	0.63
A100	0.897	0.87
A110	0.900	0.95
CES	0.892	0.53
TCS	0.898	0.59
CLS	0.895	0.65

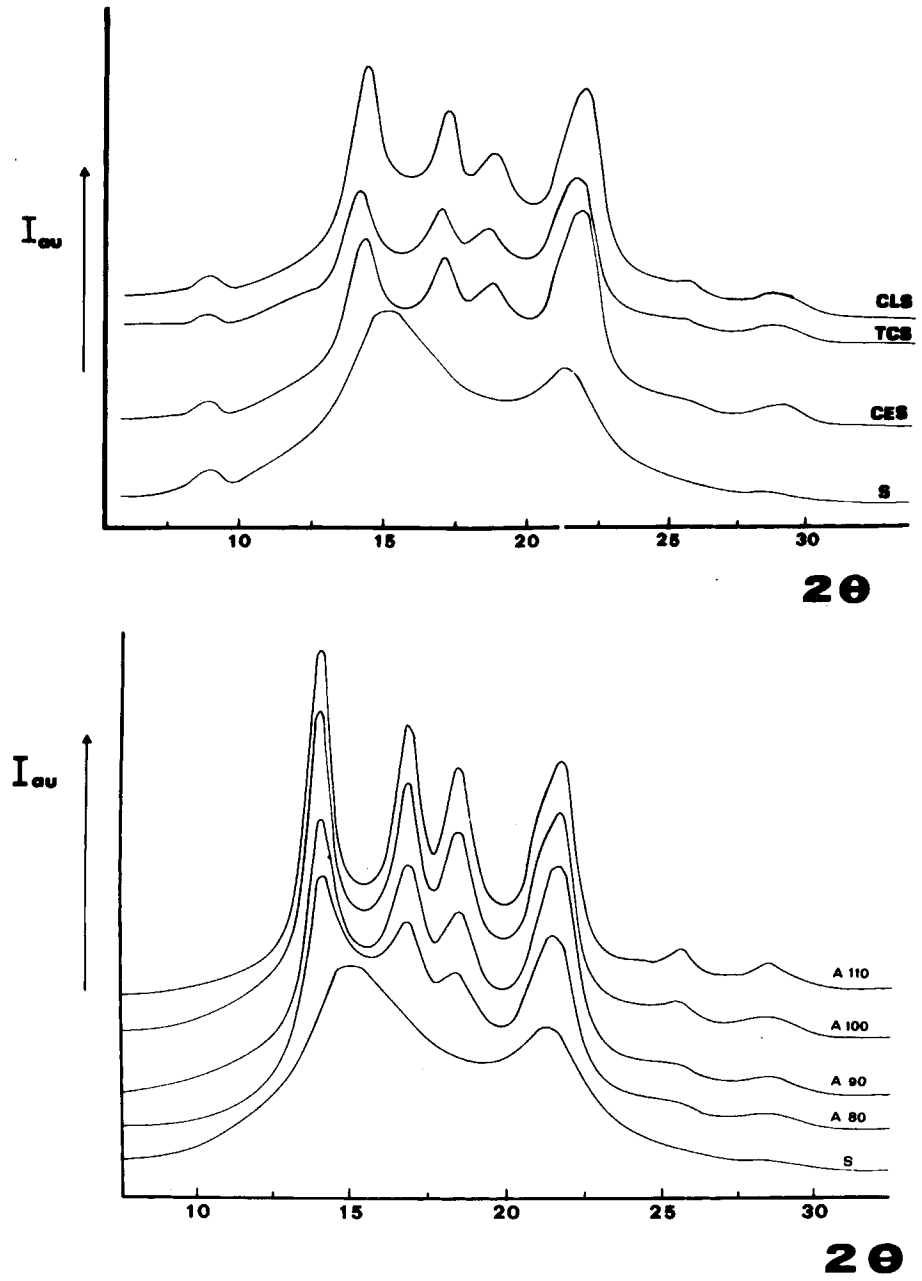

Fig. 1. Wide-angle X-ray diffractograms for sample *S* and (a) solvent-crystallized samples, (b) thermally crystallized samples. The intensity is in arbitrary units.

The starting sample *S* clearly shows the transition from the smectic phase to the normal monoclinic phase. This transition appears as an exothermic peak whose temperature is about 380°K. The exothermic transition appears also in samples A80 and A90, while it is not present in A100 and A110. This means that in A80 and A90 there is still a fraction of smectic phase, as it also

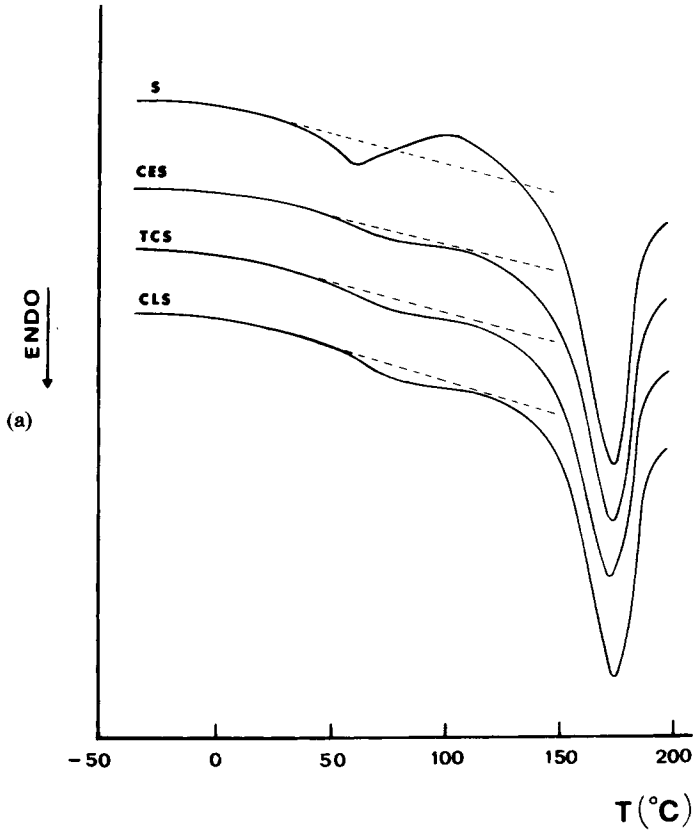

Fig. 2. DSC thermograms for samples S and (a) solvent-crystallized samples, (b) thermally crystallized samples.

emerges from the observation of their diffractograms in Figure 1. At higher temperatures the annealed samples show a small endotherm (first observed by Fichera et al.[10] and confirmed by Grebowicz et al.[8]) that starts at a temperature corresponding to the annealing temperature, and reaches a maximum at about 20° above it. According to previous interpretations, these peaks are due to small crystals of low melting temperature formed during annealing. Even sample S seems to show this endotherm but in a region of temperature in which the "upper glass transition" should appear. It is therefore doubtful if it is a real endotherm or a glass transition (masked by the starting exotherm due to the crystallization of the smectic phase). However, assuming that the endotherm peak is present also in sample S, we can speculate that it could depend on small crystals formed during the heating from quenching temperature (−70°C) to room temperature, or alternatively formed when the sample is kept at room conditions.

As for samples crystallized by SINC, that is CES, CLS, and TCS, the DSC curves do not show the first endothermic peak, indicating that this process does not lead to the formation of segregated much smaller crystalline regions, and that the distribution of the crystallite dimensions is more homogeneous. Another point worth noting is that there is no evidence of the exothermic

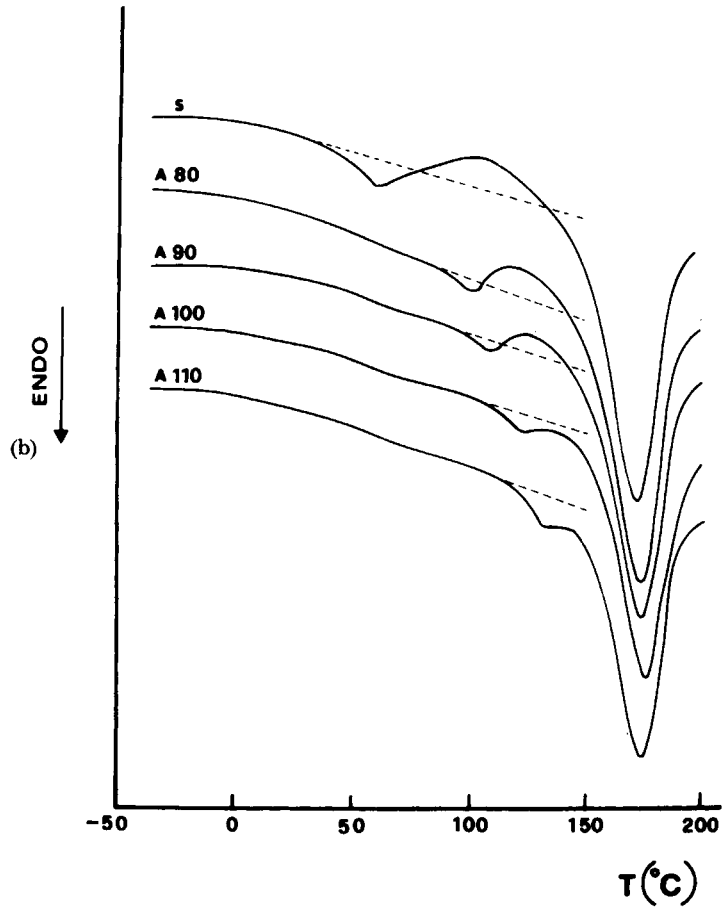

Fig. 2. (*Continued from the previous page.*)

peak (as in the samples A100 and A110 annealed at higher temperatures) indicating that the SINC was very effective in the transformation of the smectic phase.

The melting temperatures, as derived from the main melting peak, increase for all the samples on decreasing the heating rate from 50°C/min to 20°C/min. This indicates that both the thermal and the solvent induced crystallizations, produce instable crystallites that rearrange themselves during heating. This process is favored by the slower heating rate and thus we observe a higher melting temperature for the slower heating rate.

Small-Angle Light Scattering

The technique of small-angle light scattering (SALS) was used to establish the presence of spherulitic superstructures in our samples. The average size of the spherulites is determined from quantitative measurements of intensity in four-leaf-clover Hv patterns (the polarization direction of the analyzer, located behind the samples, is oriented perpendicular to the polarization direction of the incident light) according to the theory of Stein and Rhodes.[18] The average

spherulite radius R is given by

$$R = \frac{4.09\lambda}{4\pi \sin(\Theta_m/2)}$$

where λ is the wavelength of incident light and Θ_m is the scattering angle at which the maximum intensity occurs in the four equivalent lobes of the pattern.

The morphology of the quenched form of iPP was characterized by Gezovich and Geil,[19,20] who observed, in completely smectic samples, the presence of almost circular spherulites. He noted also that the more severe the quenching conditions, the greater the occurrence of isolated spherulites. In the case of the samples that we obtained at a very low temperature, we found that extremely few zones of the sample gave the four-leaf pattern (Fig. 3), from which we derived a mean spherulite diameter in the range 3 to 4 μm.

In order to determine what, if any, change in the spherulitic pattern is produced by the different treatments, a zone of the starting film showing the four-leaf pattern was annealed under the same conditions as samples A80, A90, A100, and A110. The four-leaf pattern was photographically recorded after each thermal treatment. We did not observe any change in the spherulite dimensions following annealing, as shown in Fig. 3(b) which refers to the sample annealed 30 min at 110°C. This result is in agreement with the results of Gezovich and Geil who found that annealing of a smectic sample tends to increase the monoclinic content without visibly changing the morphology.[19] A similar result was found in solvent-treated samples that do not show any change in the four-leaf pattern observed in the starting film.

Mechanical Behavior

The engineering load-elongation curves of the quenched starting iPP films (S), and thermally or solvent-crystallized samples are reported in Figure 4. They are all conventional with an upper and a lower yield point describing the neck formation and the subsequent neck propagation;[21] during the neck propagation the engineering load is constant and starts to increase when the necking is extended over all the sample. The necking phenomenon can be recorded by detecting as a function of time the local deformation in different volume elements marked on the sample. In Figure 5 the local deformation λ_L, detected in four different volume elements, is reported versus the clamps displacement λ_N, that is linearly proportional to the drawing time. Figure 5 refers to samples S and A110, and similar plots, not reported here, were obtained for the other samples. The analysis of local deformation indicates that in the neck the volume element is drawn from $\lambda_L \simeq 1.2$ to about 4–5, and the same range was observed both for the solvent-crystallized and for the annealed samples. This is in agreement with Figure 4 which shows that, starting from the lower yield point, the deformation occurs at constant load in the same range. In the neck region the morphology of the polycrystalline undrawn film is transformed into the fibrous structure of the drawn sample.[22,23] This deep morphological reorganization determines the great instability and dishomogeneity that characterizes the neck region. As soon as the neck

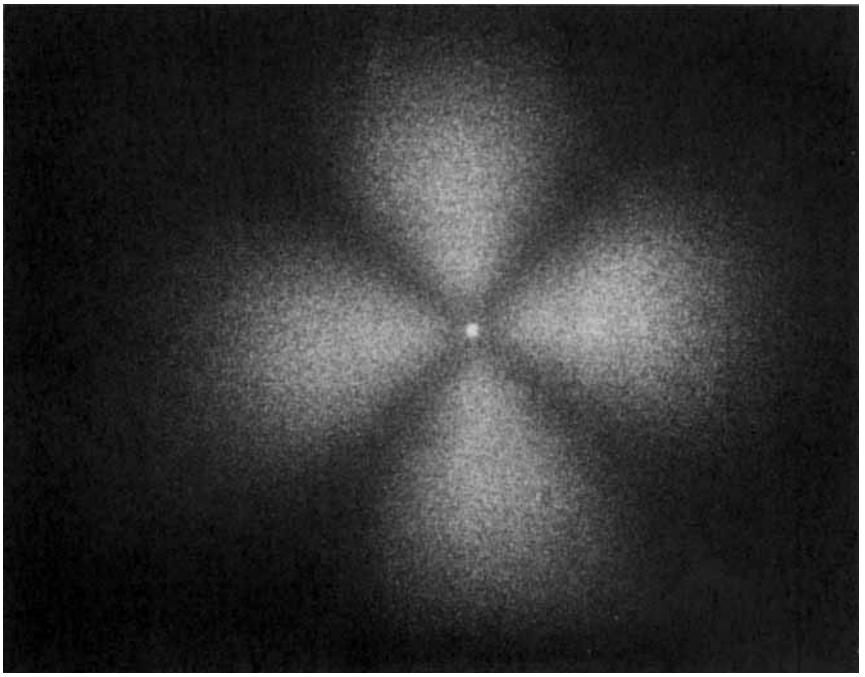

(a)

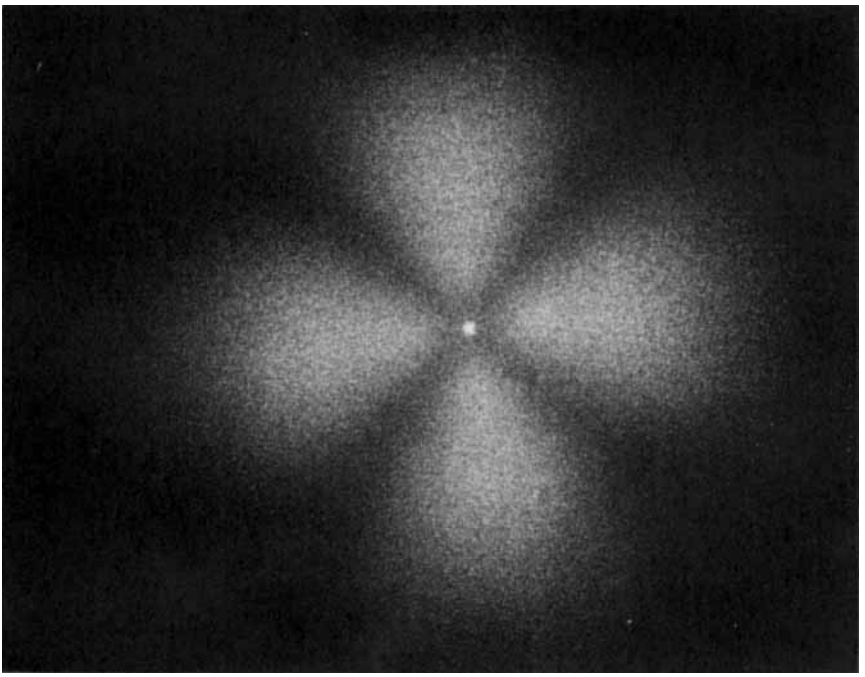

(b)

Fig. 3. H_v small-angle light scattering pattern for (a) starting sample S, (b) sample A110.

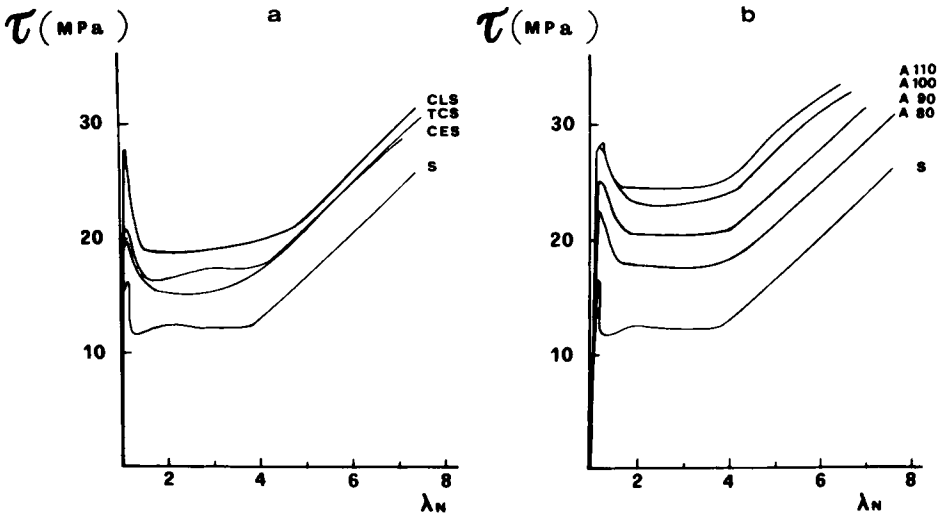

Fig. 4. The engineering load-elongation curves for sample S and (a) solvent-crystallized samples, (b) thermally crystallized samples.

reaches a volume element the deformation accelerates to a maximum rate, as can be seen in Figure 5. This rate persists during most of the transformation from the initial structure to the final fibrous one. The steadily increasing fraction of the newly formed fibrous structure gradually increases the resistance to deformation to a value above that of the undrawn film. This increase, however, takes place at a slower rate as long as there are still sections of the sample which have to be transformed into fibrous material. As soon as this transformation is completed the load starts to increase again in order to keep the total sample deformation rate the same as that imposed by the clamps displacement.

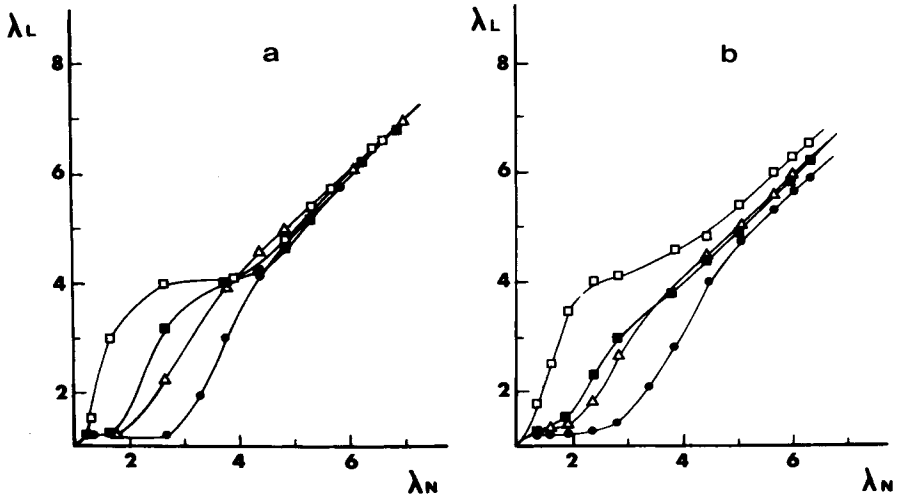

Fig. 5. The local deformation λ_L detected in four different volume elements as a function of λ_N (a) sample S, (b) sample A110.

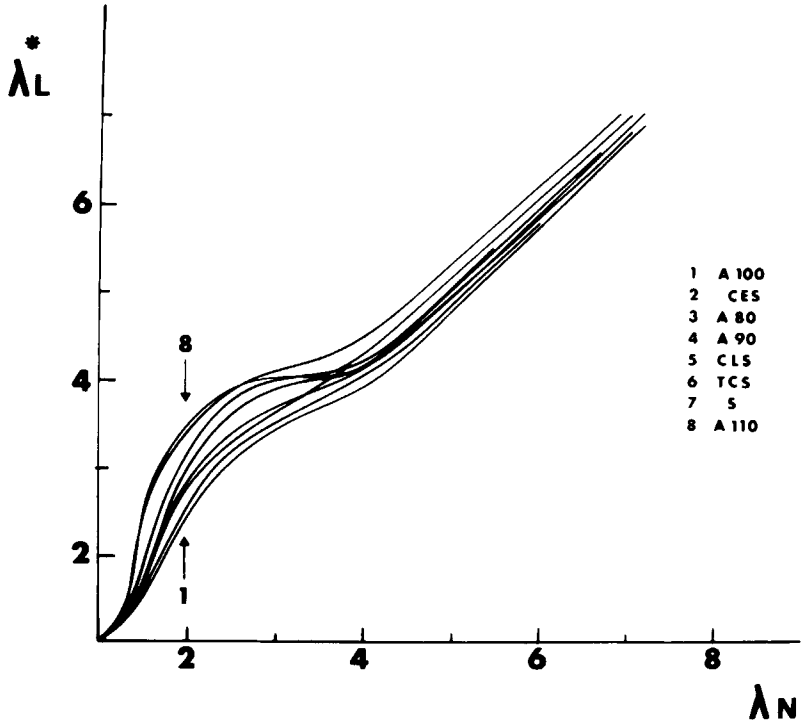

Fig. 6. The local deformation in which the virgin neck appears λ^*_L as a function of the nominal deformation λ_N. Samples from 1 to 8 are indicated in the figure.

In the range from $\lambda = 4$ to 5 to the final fracture (about 7 for all the samples) the deformation of the newly formed fibrous structure takes place. The drawing proceeds at a slower rate than in the neck, and all the volume elements are drawn at an almost identical rate. Besides these features, which are common to all the samples, it is worth noting that for samples CES, A80, A90, A100 the neck region is less sharp. The initial rate of deformation is slower for these samples even with respect to the starting sample S.

This is quite evident in Figure 6 where the deformation of the volume element in which the virgin neck appears is reported as λ^*_L versus the nominal deformation λ_N.

The true stress-strain curves, not reported here, show for all the samples that the volume elements behave in a virtually identical fashion, irrespective of the time they are subjected to necking. In fact, we obtained only one curve representing the data relative to the four zones of the sample. This demonstrates that the film and fiber structures respond to the external tensile stress in a manner characteristic of the structure but independent of the location in the sample. In Figure 7 we report the work done by the tensile force to draw the volume elements; the mechanical work in J/m^3 is reported as a function of λ_N for the different samples. All the mechanical data are reported in Table II in terms of: elastic modulus of the undrawn films E, yield point σ_y, lower yield point $\sigma_{y'}$, stress at the fracture σ_b, and draw ratio at which the fracture occurs λ_b.

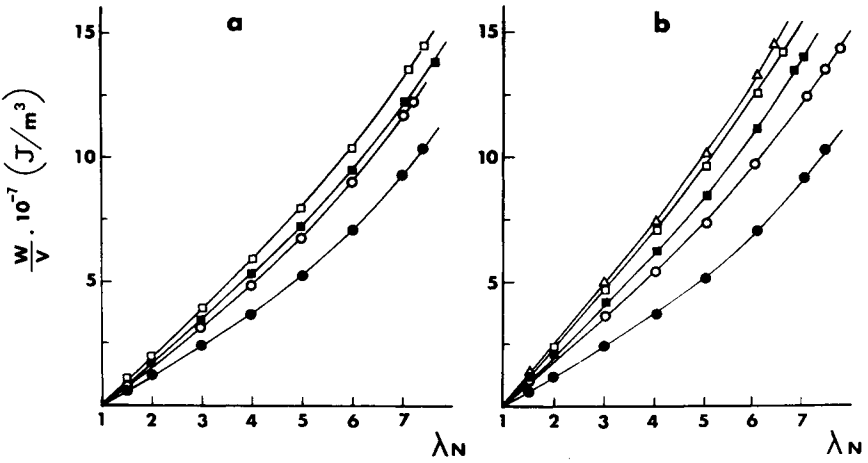

Fig. 7. The drawing mechanical work (J/m^3) as a function of λ_N for sample S (●) and (a) CES (○), TCS (■), CLS (□); (b) A80 (○), A90 (■), A100 (□), A110 (△).

TABLE II
Mechanical Parameters of the Analyzed Samples

Sample	Elastic modulus MPa	σ_y MPa	$\sigma_{y'}$ MPa	σ_b MPa	λ_b
S	600	18.3	15.3	190.1	7.4
A80	720	24.7	30.6	239.4	7.6
A90	720	30.5	36.1	218.7	6.9
A100	720	34.3	46.0	217.1	6.6
A110	690	34.0	39.4	211.1	6.3
CES	600	21.7	27.3	222.7	7.2
TCS	600	22.9	24.9	233.3	7.6
CLS	680	30.8	28.5	232.4	7.4

N.B. stress values σ_y, $\sigma_{y'}$, σ_b, are given as force on the actual cross-section.

DISCUSSION

The small-angle light scattering indicates that in sample S the spherulitic bodies that give the four-leaf pattern are segregated in very few zones. Light scattering analysis of either thermally or solvent-crystallized samples, indicates, as reported, that this morphology is fundamentally preserved, and, when detectable, also the dimension of the spherulites remains constant (see Fig. 3). On the other hand, the density and WAXD data clearly indicate a significant increase in crystallinity and order degree. This is in agreement with the conclusions of Gezovich and Geil.[19] On this basis, we can describe the analyzed drawing process as acting on a spherulitic morphology, with a crystallinity content that depends on thermal and solvent treatments. The initial spherulitic morphology is destroyed in the neck by the drastic reduction of the local section and the consequent high stress concentration. In the volume element where the macroscopic neck is visible, a high population of microneck zones is concentrated, each acting on a single morphological unit. In particular, according to Peterlin,[22,23] each spherulite generates a bundle of

microfibrils. In such morphological rearrangement, blocks of folded chains, that are the fragments of the initial structure, are displaced along the drawing axis generating the new morphological units. Therefore, in each microneck the change of the local microscopic λ is imposed directly by geometric factors, in particular the microscopic λ is the ratio between the cross-sectional areas of the initial over the final morphological units, if sections perpendicular to the stretching axis are considered. Assuming an affine deformation within the neck deformation we can extend this analysis from the microscopic to the macroscopic level, and therefore, the deformation in the macroneck must be basically equal to the microscopic λ. However, the macroneck can be more or less sharp, as shown in Figure 6. The profile of the macroscopic neck depends on the distribution profile of the microneck zones. A sharp neck is the consequence of a high, localized concentration of micronecks, while a random, diffused distribution gives rise to a less sharp profile, or to the absence of any visible macroneck. However, also in the latter case, the deformation range in which the morphological transition occurs can be identified by the stress-elongation curve. In particular, the plateau of the drawing force is indicative of the morphological transition (see Fig. 4). At the lower limit of this range the initial morphology is still present, while at the upper limit all the sample is transformed in the new fibrillar structure. Therefore, on the basis of the assumed affine deformation, the macroscopic transition range is basically correlated to the local deformation in the microneck. From this conclusion it follows that in the samples analyzed the change in the microscopic λ_L must be about 3.5 (i.e., 4 to 4.5/1.2), this ratio being constant in all the samples. Therefore, the surprising observation that the range characterized by neck propagation is practically the same in all the samples, could simply depend on the absence of significant morphological changes with the different treatments. On the other hand, the upper and lower yield points strongly depend on crystallinity, and this means that a more crystalline system opposes a higher mechanical resistance to drawing. Therefore, even if the morphology remains the same, the breaking of the spherulitic bodies, and the subsequent displacement of the fragments along the stretching direction requires a higher force. This result can be easily explained, also according to other authors,[24] considering that the increased crystallinity strongly increases the physical crosslinking and as a consequence strongly increases the internal viscosity of the system. The complex structural and molecular rearrangement that characterizes the transition from spherulitic to fiber morphology is strongly hindered by the increased number of permanent intermolecular contacts generated by the crystallization process.

A similar explanation can be given for the data in Figure 7, where the mechanical work is reported as a function of λ. The work increases in the thermally crystallized samples in agreement with the density and WAXD data, while in the solvent crystallized samples the agreement regards the WAXD data only. However for the TCS sample the density value, as suggested, might be affected by residual solvent entrapped in the newly formed crystalline structure. The mechanical behavior indicates that this explanation is the more reliable one.

To conclude, a comment on fracture behavior. Figure 4 shows that λ_b is fundamentally constant in the solvent-treated samples, while a small decrease

in λ_b can be observed on increasing the annealing temperature. Anyway the effect is not important. Considering that the fracture mechanism is mainly driven by the inter microfibrillar taut tie molecules, as exhaustively explained in a previous paper,[25] we can speculate that the local stress acting on these molecules must be basically the same in the different samples. The fracture occurs at a total stress that increases with the crystallinity, but in the microscopic scale the increase is mainly intramicrofibrillar, while the intermicrofibrillar tension is not significantly different in the different samples. This possibility is in good agreement with the parallel coupling of the different microfibrils that is compatible with a nonhomogeneous distribution of the stress on the cross-section.

The authors wish to thank Dr. A. Segre (C.N.R.-Rome) for the NMR analysis and useful discussions.

References

1. G. Natta, M. Peraldo, and P. Corradini, *Rend. Acc. Naz. Lincei*, **26**, 14 (1959).
2. R. L. Miller, *Polymer* **1**, 135 (1960).
3. H. D. Keith, F. J. Padden, N. M. Walter, and H. W. Wyckoff, *J. Appl. Phys.* **30**, 1485 (1959).
4. P. B. McAllister, T. J. Carter, and R. M. Hinde, *J. Polym. Sci. Phys.*, **16**, 49 (1978).
5. G. Bodor, M. Grell, and A. Kello, *Faser Forsch. Text. Technol.* **15**, 527 (1964).
6. R. Zanetti, G. Celotti, A. Fichera, and R. Francesconi, *Makrom. Chem.*, **128**, 137 (1969).
7. B. Wunderlich and J. Grebowicz, *J. Adv. Polym. Sci.*, **60 / 61**, 1 (1984).
8. J. Grebowicz, J. F. Lau, and B. Wunderlich, *J. Polym. Sci. Symp.*, **71**, 19 (1984).
9. P. J. Hendra, J. Vile, H. A. Willis, V. Zichy, and M. E. A. Cudby, *Polymer*, **25**, 785 (1984).
10. A. Fichera, and R. Zannetti, *Makromol. Chem.*, **176**, 1885 (1975).
11. V. Vittoria and F. Riva, *Macromolecules* **19**, 1975 (1986).
12. L. Rebenfeld, P. J. Makarewicz, H. D. Weighmann, and G. L. Wilkes, *J. Macromol. Sci. Rev. Macromol. Chem.*, **C15** (2), 279 (1976).
13. A. B. Desai and G. L. Wilkes, *J. Polym. Sci. Symp.*, **46**, 291 (1974).
14. P. J. Makarewicz and G. L. Wilkes, *J. Appl. Polym. Sci.*, **22**, 3347 (1978).
15. P. J. Makarewicz, G. L. Wilkes, and Y. Budnitsky, *J. Polym. Sci. Phys.*, **16**, 1545 (1978).
16. V. Vittoria, *J. Polym. Sci. Phys.* **24**, 651 (1986).
17. L. E. Alexander, *X-Ray Diffraction Methods in Polymer Science*, J. Wiley-Interscience, New York, 1969.
18. R. S. Stein and M. B. Rhodes, *J. Appl. Phys.*, **31**, 1873 (1960).
19. D. M. Gezovich and P. H. Geil, *Polym. Eng. Sci.*, **8**, 202 (1968).
20. D. M. Gezovich and P. H. Geil, *Polym. Eng. Sci.*, **8**, 212 (1969).
21. L. E. Nielsen, *Mechanical Properties of Polymers and Composites*, Marcel Dekker Inc., New York and Basel.
22. A. Peterlin, *J. Polym. Sci.*, **C9**, 61 (1965).
23. A. Peterlin, *Ultra High Modulus Polymers*, A. Ciferri and I. M. Ward, Eds., Applied Science, Barking, England, 1979.
24. G. Capaccio, A. G. Gibson, and I. M. Ward, *Ultra High Modulus Polymers*, A. Ciferri and I. M. Ward, Eds., Applied Science, Barking, England, 1979.
25. F. de Candia, R. Russo, V. Vittoria, and A. Peterlin, *J. Polym. Sci.*, **20**, 269 (1982).

Received June 24, 1986
Accepted September 19, 1986